IET Generation, Transmission & Distribution

Research Article

IET Journals
The Institution of Engineering and Technology

Voltage–current technique to identify fault location within long transmission lines

ISSN 1751-8687
Received on 19th May 2020
Revised 24th July 2020
Accepted on 1st September 2020
E-First on 19th October 2020
doi: 10.1049/iet-gtd.2020.1012
www.ietdl.org

Ahmed Abu-Siada[1] ✉, Mohamed I. Mosaad[2], Saif Mir[1]

[1]*Curtin University, Western Australia, Australia*
[2]*Yanbu Industrial College (YIC), Yanbu, Kingdom of Saudi Arabia*
✉ *E-mail: a.abusiada@curtin.edu.au*

Abstract: Current industry practice to identify fault location in transmission lines is based on visual inspection, travelling waves, and line impedance measurement. Unfortunately, these techniques are only developed to detect the fault location upon its occurrence without the ability to predict abnormal events that usually precede major faults and issue a timely warning signal to avoid potential consequences for power line failures. Furthermore, the current fault locating techniques exhibit some drawbacks that limit their wide practical implementation. This includes cost, access to required data, and low accuracy when employed for specific power line topologies. This study is aimed at presenting and validating a new cost-effective technique based on the line voltage–current characteristics to predict and identify the location of various abnormal and fault events in real-time. By measuring the currents and voltages at both ends of the line, a unique line fingerprint can be identified. Any change in this fingerprint can be detected and analysed by a software installed in the control centre in real-time to identify the location, type, and level of the abnormal events or emerging faults. Robustness of the proposed technique is assessed through simulation analysis conducted on various case studies along with a practical case study.

1 Introduction

Overhead power lines are vital links in electrical transmission and distribution networks. As they are usually operating under harsh environmental conditions, power lines are subjected to abnormal events such as wind gusts, snow accumulation, lightning, birds' activities, and falling trees [1, 2]. Such events may lead to conductor swinging followed by short circuit faults. While no technique has so far been developed to accurately identify such abnormal events and hence predict faults before their occurrence, several techniques have been developed to identify fault locations within power lines. These techniques include travelling waves and apparent impedance methods [3, 4]. The visual aerial method may also be utilised, however, due to the high cost and risk involved, this method is used every 3 to 5 years for line condition assessment [5]. The travelling wave method identifies fault location based on the speed of the surge signals that appear at the fault location and propagate over the line in both directions along with the time it reaches the measuring location [6]. The fault location (m), measured from one terminal of the line is calculated using (i) for single-ended and (ii) for double-ended travelling wave-based methods [7]

$$m = \frac{1}{2}(t_1 - t_2) \cdot v \tag{1}$$

$$m = \frac{1}{2}(l + (t_1 - t_3) \cdot v) \tag{2}$$

where l is the length of the line, v is the speed of propagation, t_1 and t_2 are, respectively, the arrival times of the first incident wave and reflected wave from the fault location measured at the same local terminal of the line, and t_3 is the arrival time measured at the other remote terminal of the line.

The key challenge for travelling wave-based methods is that the initial transient must be captured using a very precise time tagging device for accurate fault locating [8]. Furthermore, as travelling waves reflect at discontinuity points, e.g. in the case of two connected lines of different characteristic impedances or hybrid line/cable connection, identification of the correct signal is critical. Travelling waves may also be generated during normal line operation as a result of switching operations and lightning strikes thus identification of the exact signal related to the fault becomes a challenging task. The accuracy of the travelling wave method is affected by the stiffness of the transmission network, line length, and assumed propagation speed. Implementation of the travelling wave method calls for expensive high-frequency sampling fault locating device installed at one or two terminals of the line [9].

In the impedance-based method, fault location is identified based on the ratio of the measured reactance to the total reactance of the transmission line (TL) [7]. A calculation error arises when the fault and source currents are not in phase. This error can be reduced by adopting some modified techniques such as Tagaki, Eriksson, and double-ended-based methods [10, 11]. However, impedance-based methods call for precise information about the source and line impedances and a significant error is introduced to the calculations when the fault impedance is not a constant value. Furthermore, when impedance-based methods are implemented on three-terminals or tapped lines, inaccurate calculations may arise especially in the case of series compensated and un-transposed lines. The above-mentioned two techniques can be implemented on single or double terminals data-based methods. In the case of double terminals techniques, the communication protocol between the two terminals of the line such as satellite global positioning system (GPS) and phase measurement units (PMUs) at both terminals are to be used [12]. In general, the accuracy of current fault locating techniques may be affected by load impedance dynamics, fault impedance, mutual coupling between parallel lines, power quality, line configuration, line compensation, and saturation of current and potential transformers [7].

This paper is taking one step forward in validating the feasibility of the technique that was introduced in [13]. The technique is based on identifying a unique voltage–current characteristic (fingerprint) for each line whereas any deviation from this fingerprint due to emerging faults or abnormal events within the line can be detected in real-time so that a proper action can be taken to avoid any potential consequences. While the concept of the technique is presented for the first time in [13], further feasibility study on different line topologies, complex interconnected power systems along with a practical case study are

© The Institution of Engineering and Technology 2020

Authorized licensed use limited to: Electricity Generating Authority of Thailand. Downloaded on November 09,2020 at 08:24:32 UTC from IEEE Xplore. Restrictions apply.

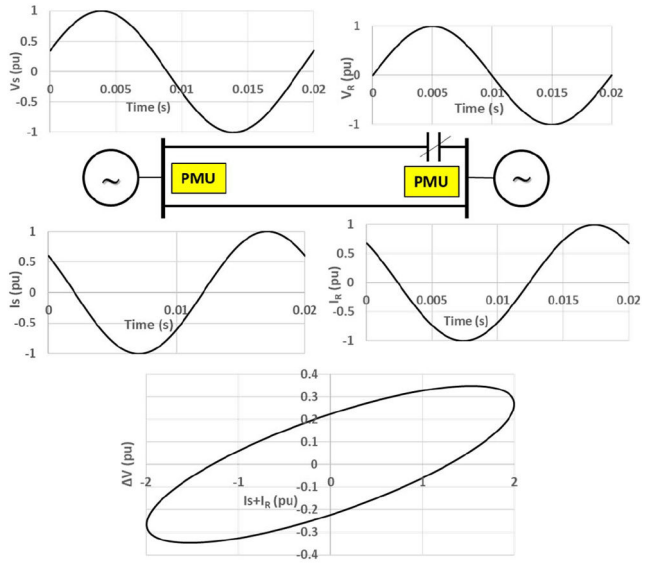

Fig. 1 *Graphical illustration of the proposed approach*

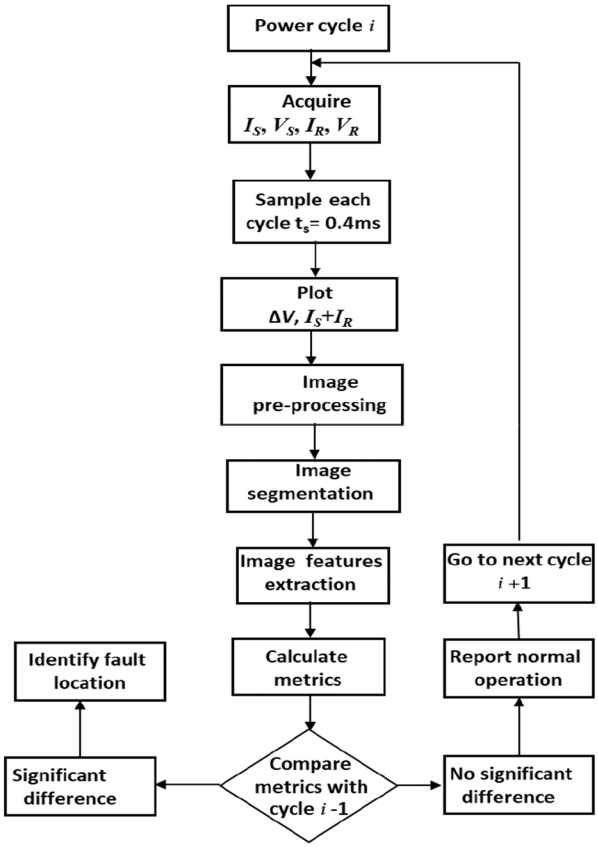

Fig. 2 *Flow chart of the proposed technique*

presented in this paper. The accuracy of the technique to detect faults within compensated lines as well as detecting abnormal events due to high-impedance faults is also investigated. Correlation between fault/abnormal event location and the proposed line characteristic is investigated using the digital image processing (DIP) approach.

2 Proposed technique and DIP

The proposed fingerprint is a relation between the voltage difference at both terminals of the line and the summation of the currents at both sides as shown in Fig. 1.

Fig. 1 shows that the currents and voltages at the sending (I_S, V_S) and receiving (I_R, V_R) ends are to be measured using PMU installed at both ends of the line. The data can be synchronised using GPS time reference at both ends. As shown in Fig. 1, the locus of $\Delta V = V_S - V_R$ and $I_S + I_R$ represents an ellipse whose geometrical dimensions depend on the currents and voltages at both ends [14, 15]. It is worth mentioning that the ellipse may exhibit changes due to normal dynamic operation and transient events. However, these changes can be easily discriminated from the changes due to fault conditions as presented in [13]. DIP techniques enhance the analysis of graphic plots such as the elliptic plot shown in Fig. 1 using electronic devices. To automate the fault identification process, the proposed graphical fingerprint is represented by a two-dimensional matrix $[\boldsymbol{A}]_{X \times Y}$ consists of a finite number of pixels. Each pixel on the proposed image is represented mathematically as $a(x_1, y_1)$ with an image intensity $|a|$ at a spatial location (x_1, y_1) with respect to X–Y coordinates [16]. While in this paper, only geometrical features of the proposed line fingerprint are considered, other DIP features such as invariant moments and texture analysis can be extracted to increase the accuracy of the proposed technique [17]. The methodology of the proposed technique is shown in Fig. 2.

The process starts by acquiring the required data from both terminals of each phase of the TL (I_S, V_S, I_R, V_R). The measured data are to be sampled over one complete power cycle using a sampling time of 0.4 ms, which is the typical sampling rate of the PMU. These sampled parameters are used to construct the proposed voltage–current characteristic of each phase at every power frequency cycle (20 ms for 50 Hz networks). Image pre-processing is conducted to resize the image, adjust its colour and extension type to facilitate accurate image detection using electronic systems [18]. The segmentation process divides the pre-processed image into several segments to identify the actual image characteristics and eliminate noise and background using the optimal multistage Canny edge detection algorithm [18–20]. Following the above steps, various unique image features such as geometric dimensions can be extracted [21]. These features are used to calculate three classification metrics; root mean square (RMS) at each power cycle, city-block distance (CBD); the absolute difference between a pair of features, and image Euclidean distance (IED); the straight-line distance between two features at two consecutive power cycles. These classification metrics are compared with the corresponding ones calculated at a previous power cycle to identify any anomalies. In case of significant metrics deviation from one cycle to another, an abnormal event is to be reported at the control centre. Based on the extracted image features, fault or abnormal location can be identified as elaborated below.

The extracted physical dimensions include entire area of the ellipse g_1, ellipse minor and major axes lengths (g_2 and g_3) and ellipse focus point (g_4). These parameters can be calculated using the following equations [22]:

$$g_1 = \sum_{x=0}^{X-1} \sum_{y=0}^{Y-1} a(x, y) \tag{3}$$

$$g_2 = \sqrt{(x_1^2 + x_2^2) - f^2} \tag{4}$$

$$g_3 = x_1 + x_2 \tag{5}$$

$$g_4 = \sqrt{\left(\frac{g_3}{2}\right)^2 - \left(\frac{g_2}{2}\right)^2} \tag{6}$$

where $a(x, y)$ is the image intensity at a spatial location x, y; x_1 and x_2 represent the distance from each of the two ellipse foci to any point on the ellipse contour and f is the distance between the two foci.

The extracted n-features are used to calculate the above-mentioned three metrics as below [23]

$$\text{CBD} = \sum_{j=1}^{n} \left| f\,\text{cycle}(i)\text{feature}_j - \text{cycle}(i+1)\text{feature}_j \right| \tag{7}$$

© The Institution of Engineering and Technology 2020

Authorized licensed use limited to: Electricity Generating Authority of Thailand. Downloaded on November 09,2020 at 08:24:32 UTC from IEEE Xplore. Restrictions apply.

$$\text{RMS} = \sqrt{\frac{1}{n}\sum_{j=1}^{n}\text{feature}_j^2} \tag{8}$$

$$\text{IED} = \sqrt{\sum_{j=1}^{n}\left(\text{cycle}\,(i)\text{feature}_j - \text{cycle}\,(i+1)\,\text{feature}_j\right)^2} \tag{9}$$

3 Investigated system and case studies

Fig. 3 shows a modified version of the single line diagram for system-2 of the IEEE second benchmark model for computer simulation of sub-synchronous resonance [24]. The two 50 Hz, 100 MVA generators at bus bars 1 and 2 are connected through two parallel 150 km, 500 kV TLs of which one is compensated using a series capacitor (X_c). To carry out the investigations in this paper, this system is simulated using Matlab/Simulink software.

As a single line to ground (L–G) fault represents about 70% of TL faults, a single line (phase-A) to ground fault is simulated at different locations of TL1 of the system under study. The proposed line characteristic is obtained by measuring the phase voltages and currents at bus-1 (V_S, I_S) and bus-2 (V_R, I_R). The measured sinusoidal waveforms are sampled over one complete cycle as discussed above to plot the proposed locus (ΔV versus $I_S + I_R$) in per unit (pu) of the nominal rated power and voltage (100 MVA, 500 kV) for each case study. The location of fault (m in km) is measured from bus-2 as shown in Fig. 3.

3.1 Line fingerprint and reference features

During normal operation of the network shown in Fig. 3, the collected data at buses 1 and 2 are used to plot the proposed fingerprint of the three phases of TL1 without and with the series capacitor (50% compensation ratio is considered in this case) as shown in Figs. 4*a* and *b*, respectively.

It can be seen from Fig. 4 that the proposed characteristics for the three phases are identical during normal operation. The increment of the current in the case of the compensated line is attributed to the decrease in the line overall reactance. The simulation results in Fig. 4 are manipulated using the developed DIP code to extract the above-mentioned four geometrical dimensions along with the angle θ between the ellipse major axis and the x-axis as listed in Table 1. These features are considered as reference data set for the line without and with capacitor series compensation.

3.2 Single phase to ground fault for uncompensated line

In this case study, a bolted L–G fault is simulated at different locations of phase-A of TL1 when no series compensation is employed. The obtained elliptic plots at different fault locations are compared with the line fingerprint as shown in Fig. 5.

It can be seen from Fig. 5 that when L–G fault takes place in the middle of the line (75 km), the proposed locus does not encounter significant rotation. However, the ellipse entire area decreases slightly when compared with the healthy fingerprint. When the fault occurs at locations <75 km (measured from bus-2), the ellipse rotates in an anticlockwise direction with a significant increase in the entire area. Ellipse rotation and area are more pronounced when the fault becomes closer to bus-2. On the other hand, when the fault occurs at a location >75 km, mirrored elliptic plots are attained, i.e. the locus obtained due to a fault at 125 km is almost similar to the obtained locus due to a fault at 25 km but in the opposite direction. The extracted physical dimensions of the obtained results along with the angle of rotation of the major axis θ are listed in Table 2.

The extracted features in Table 2 show that each fault location within the uncompensated line will have a unique impact on the proposed line V–I characteristic. Results also reveal that the effect of L–G fault in the middle of the line can be taken as a reference in terms of ellipse rotation.

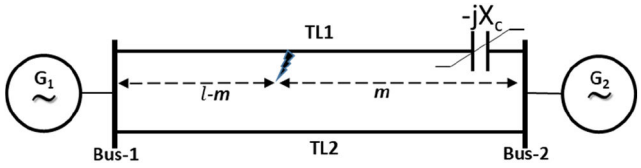

Fig. 3 *Single line diagram for the TL network under study*

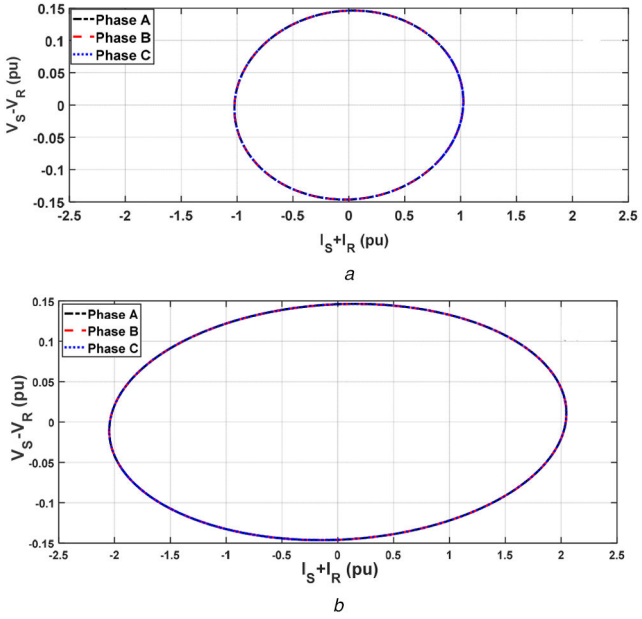

Fig. 4 *Fingerprint for the three phases of TL1*
(a) Without series compensation, ***(b)*** With 50% series compensation

Table 1 Reference geometrical dimensions for the investigated TL in Fig. 3

Feature	Without compensation	With 50% compensation
g_1	0.47	0.94
g_2	0.29	0.29
g_3	2.05	4.09
g_4	1.01	2.04
θ	0.34	0.31

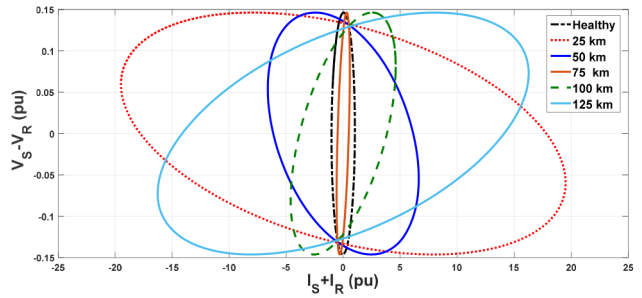

Fig. 5 *Single L–G fault at different locations (no compensation)*

3.3 Single phase to ground fault for compensated line

The above case study is repeated when the line is compensated with a compensation ratio ($X_C/X_L = 50\%$). The results of this case study are shown in Fig. 6 with geometrical dimensions listed in Table 3. Fig. 6 and Table 3 reveal that with capacitor series compensation close to bus-2, the proposed line characteristic exhibits a rotation in an anti-clockwise direction with a maximum effect on the entire area and major axis length when the fault takes place at the middle of the line, which may be attributed to the unsymmetrical impedance seen by the mid-point from both sides of the line.

© The Institution of Engineering and Technology 2020

Authorized licensed use limited to: Electricity Generating Authority of Thailand. Downloaded on November 09,2020 at 08:24:32 UTC from IEEE Xplore. Restrictions apply.

Table 2 Geometrical dimensions for bolted L–G fault at different locations (no compensation)

Feature	25 km	50 km	75 km	100 km	125 km
g_1	8.19	2.82	0.23	1.76	6.49
g_2	0.27	0.27	0.25	0.24	0.25
g_3	39.01	13.23	1.17	9.22	32.56
g_4	19.50	6.16	0.57	4.61	16.28
θ	−0.18	−0.47	8.00	1.01	0.25

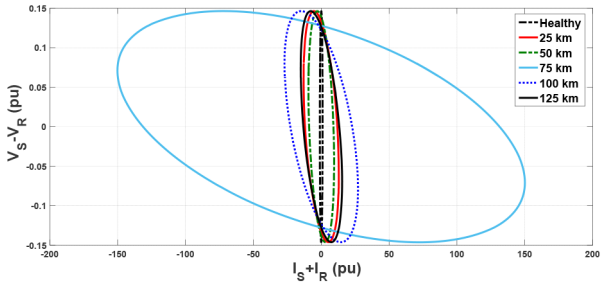

Fig. 6 *Single L–G fault at different locations (50% compensation)*

Table 3 Geometrical dimensions for bolted L–G fault at different locations (with 50% compensation)

Feature	25 km	50 km	75 km	100 km	125 km
g_1	5.46	2.82	60.38	10.51	6.17
g_2	0.27	0.27	0.26	0.25	0.26
g_3	26.13	13.23	300.32	54.16	30.75
g_4	13.07	6.62	150.16	27.08	15.37
θ	−0.26	−0.47	−0.03	−0.17	−0.27

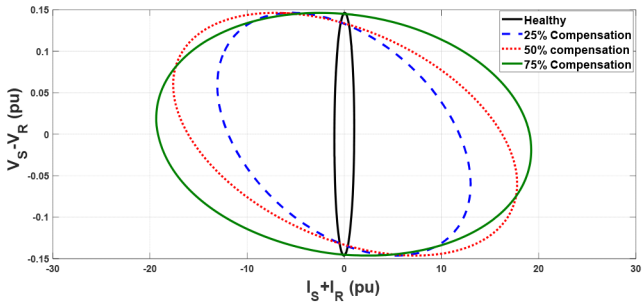

Fig. 7 *Single L–G fault at 25 km with different compensation ratios*

Table 4 Geometrical dimensions for bolted L-G fault at different compensation ratios ($m = 25$ km)

Feature	25%	50%	75%
g_1	5.46	7.47	8.82
g_2	0.27	0.27	0.29
g_3	26.13	35.57	38.71
g_4	17.79	13.07	19.35
θ	−0.26	−0.19	−0.05

3.4 Effect of compensation ratio

The above case study shows that when the line is compensated using a series capacitor connected to one end, the effect of L–G fault on the proposed ellipse at each fault location is different than the case of uncompensated line. To investigate the effect of compensation ratio on the proposed line characteristic, a bolted L–G is applied at $m = 25$ km and the proposed ellipse is plotted for three compensation ratios (25, 50, and 75%) as shown in Fig. 7. It is to be noted that the healthy plot in Fig. 7 is obtained for a 50% compensated line with no fault.

Fig. 7 reveals that a faulty compensated line enforces the ellipse to rotate in an anticlockwise direction with a substantial increase in the entire area. This effect is more pronounced when the compensation ratio increases as can be seen from the extracted geometrical features in Table 4.

3.5 Discontinuity in the line characteristic impedance

One of the main drawbacks of the travelling wave-based fault locating technique is when there is a discontinuity in the line characteristic impedance. For instance, when an overhead line is connected to a substation transformer through a short cable to suppress ferroresonance and lightening impacts. A cable also may be connected to the overhead TL at some sections due to right of way issues, or the nature of terrestrial [25]. To investigate the effect of such a hybrid connection on the proposed method in this paper, a feeder of 5 km length and characteristic impedance 10% of the line characteristic impedance is connected between TL1 and bus-2 in Fig. 3. The results of this case study are obtained for an uncompensated line and when the line comprises a 50% compensation ratio as shown in Figs. 8 and 9, respectively. Results in Fig. 8 reveal almost the same effect on the proposed characteristics of the fault taking place on a line with no cable connected (Fig. 5).

When the line-cable configuration is compensated (Fig. 9), the effect of L–G fault on the proposed ellipse is also similar to the effect of the fault on the compensated line with no cable connection (Fig. 6). The extracted images features of this case study are listed in Tables 5 and 6. These results attest to the advantage of the proposed technique over the travelling wave-based method in such a line-cable configuration.

3.6 Detection of abnormal events

One of the key features of the proposed technique is its ability to detect abnormal events and high-impedance faults. To assess this feature, a single L–G fault is applied in the middle of TL1 ($m = 75$ km). Various high-impedance faults (1, 2.5, 4, and 6 kΩ) are simulated and the proposed line characteristic is obtained at each fault impedance as shown in Fig. 10 with image features and fault current at each fault impedance as listed in Table 7.

© The Institution of Engineering and Technology 2020

Authorized licensed use limited to: Electricity Generating Authority of Thailand. Downloaded on November 09,2020 at 08:24:32 UTC from IEEE Xplore. Restrictions apply.

Fig. 10 and Table 7 show that the proposed line characteristic will be impacted even when the fault impedance is 6 kΩ with a very small fault current that cannot be detected through the protection relays. While the impact of such high-impedance faults on some parameters such as ellipse entire area and minor axis length when compared with the corresponding features of normal line operation is not significant, the effect on the major axis length, focus point, and angle of rotation is noticeable. This implies the key role this technique may play in detecting abnormal events in the transmission and distribution networks prior to fault occurrence so that timely action can be taken to avoid catastrophic consequences.

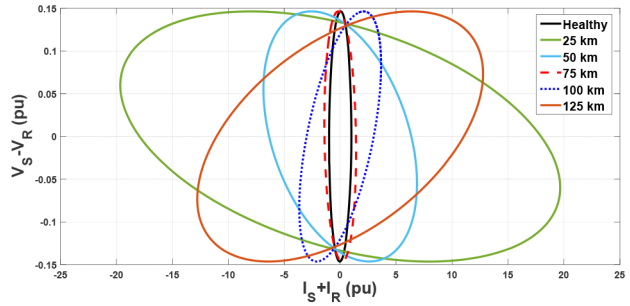

Fig. 8 *Single L–G fault at different locations of line cable connection (without compensation)*

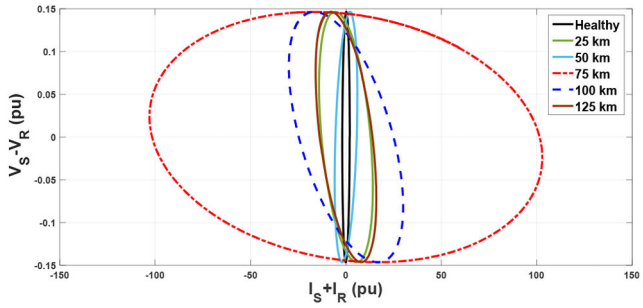

Fig. 9 *Single L–G fault at different locations of line cable connection (with 50% compensation)*

3.7 Effect of series-capacitance location

Usually, the compensation for transmission networks is placed at the terminals of the line for easy maintenance. In some long lines, a compensation can be also placed close to the middle of the line. To investigate the impact of the location of the series-capacitance compensation on the proposed line characteristics, a bolted single L–G fault is applied at $m = 50$ km. The V–I characteristic of the line is plotted for three locations of the series capacitance; left and right of the line (bus-1 and bus-2, respectively) and at the middle of the line as shown in Fig. 11. Results show that the line V–I characteristic is changing based on the location of the series capacitor especially the angle of rotation. It can also be observed that when the series capacitor is placed at either terminal of the line mirrored ellipses are obtained for a single L–G fault close to the middle of the line which is attributed to the almost symmetrical impedance seen by each bus in this case.

3.8 Effect of shunt reactor

The above analysis assumed series-capacitor compensation only for the TL. Shunt reactor compensation may also be used to improve the voltage profile of the TL and to control the overall compensation ratio. To investigate the impact of shunt-reactor compensation on the proposed TL V–I characteristic, a shunt reactor is connected to bus-2 of the investigated system. The fingerprint (with no fault) is plotted for TL1 with no compensation, 50% series-capacitor compensation, shunt-reactor compensation, and with series–shunt compensation connected to bus-2. As shown in Fig. 12, series compensation affects the proposed line characteristic through enlarging the entire area of the ellipse with almost no rotation when compared with the line characteristic with no compensation. Shunt reactor compensation on the other hand

Table 5 Geometrical dimensions for bolted L–G fault at different locations of line-cable (no compensation)

Feature	25 km	50 km	75 km	100 km	125 km
g_1	8.25	2.92	0.65	1.39	5.08
g_2	0.27	0.27	0.29	0.24	0.25
g_3	39.33	13.73	2.84	7.32	25.56
g_4	19.67	6.86	1.41	3.66	12.78
θ	−0.17	−0.46	−0.71	1.31	0.33

Table 6 Geometrical dimensions for bolted L-G fault at different locations of line-cable (50% compensation)

Feature	25 km	50 km	75 km	100 km	125 km
g_1	5.96	2.55	46.71	11.49	6.43
g_2	0.27	0.27	0.29	0.24	0.25
g_3	28.25	11.92	206	59.95	32.41
g_4	14.13	5.96	103	29.97	16.21
θ	−0.25	−0.46	−0.01	−0.13	−0.28

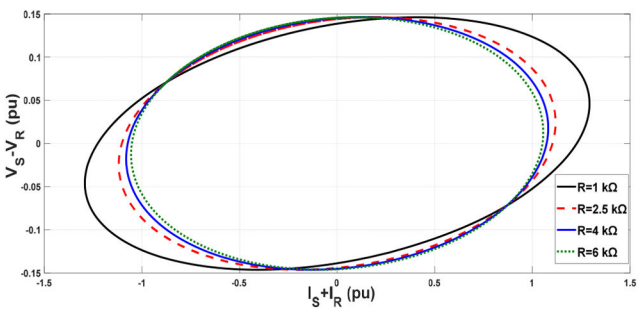

Fig. 10 *Impact of fault impedance on the proposed method (no compensation)*

© The Institution of Engineering and Technology 2020

Authorized licensed use limited to: Electricity Generating Authority of Thailand. Downloaded on November 09,2020 at 08:24:32 UTC from IEEE Xplore. Restrictions apply.

Table 7 Geometrical dimensions for high impedance L-G fault at the middle of the line (no compensation)

Feature	Normal	1 kΩ	2.5 kΩ	4 kΩ	6 kΩ
g_1	0.47	0.56	0.51	0.49	0.48
g_2	0.29	0.28	0.29	0.29	0.29
g_3	2.05	2.59	2.24	2.16	2.11
g_4	1.01	1.29	1.11	1.07	1.05
θ	0.34	2.08	1.35	0.96	0.69
fault current	—	50 A	23 A	9 A	3 A

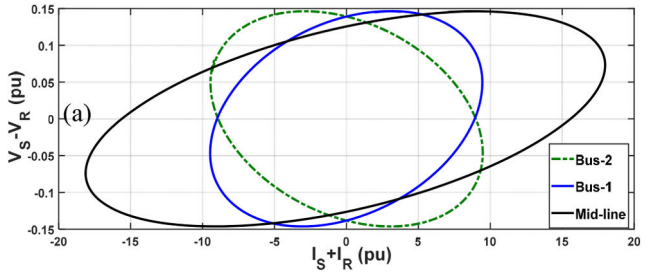

Fig. 11 *Single L–G fault at 50 km of TL1 with series-capacitance compensation at different locations*

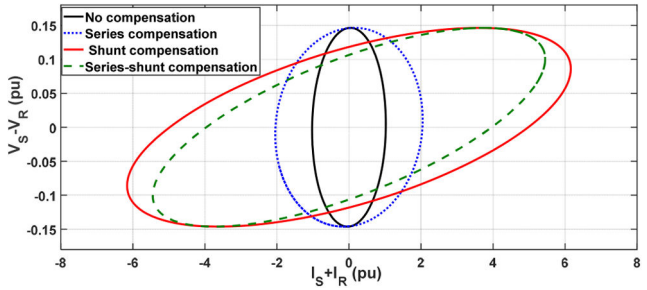

Fig. 12 *Line fingerprint with no compensation, series, shunt, and series–shunt compensations*

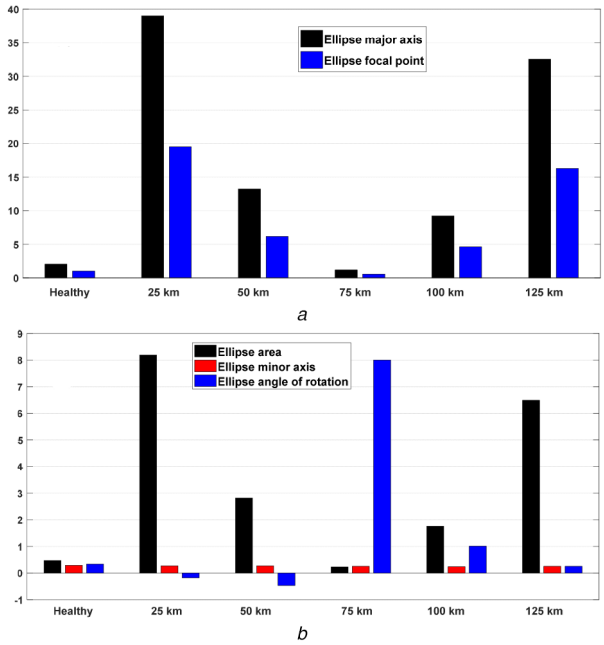

Fig. 13 *Impact of L–G fault at different locations on various features of the proposed line characteristic*
(a) Major axis and focal point, ***(b)*** Area, minor axis, and angle of rotation

results in a significant increase of the ellipse entire area with observable rotation in the clockwise direction which is the same effect of series–shunt compensation with a slight reduction in the major axis length. The increased current due to shunt compensation is attributed to the reduction of the entire impedance seen by both buses.

It is to be noted that the proposed technique is based on a relative comparison with the line fingerprint that may differ from line to another based on several factors including the type, location, and level of the compensation. The technique is comparing the measured *V–I* characteristic of a particular line with its unique fingerprint to detect any anomalies in real-time as discussed above.

4 Classification metrics and fault location

This section presents a numerical technique to identify the L–G fault location within a TL based on the simulation results of Fig. 5 and Table 2. Fig. 13 shows a comparison of all extracted features at each fault location with the corresponding ellipse features during line normal (healthy) operation. From Fig. 13, it can be concluded that

- The ellipse entire area increases significantly when the fault occurs close to the two ends of the line while it is slightly affected when the fault takes place in the middle of the line. The impact of fault on the ellipse area can be approximated by a parabola with an axis of symmetry passes through a vertex located at the midpoint of the line.
- The minor axis length slightly decreases due to the L–G fault and it is hard to distinguish faulty cases and identify fault location using this parameter.
- The ellipse major axis length encounters the same effect as the ellipse entire area and an observable parabolic trend can be approximated using this parameter as well.
- The angle of rotation exhibits two directions clockwise when the fault occurs at or to the right of the line midpoint (75 km) and anticlockwise, when the fault takes place at the left of the line midpoint. While it is hard to distinguish the fault at the midpoint from the healthy characteristics using the above parameters (area, focus point, minor, and major axes), the angle of rotation can be used to identify the fault at the middle of the line. As mentioned in the introduction section, the accuracy of this technique can be increased by extracting more image features such as invariant moments and texture analysis.

Three classification metrics are calculated based on the extracted features using (7)–(9) and are listed in Table 8. Results show that the RMS value for the normal line operation can be employed as a threshold limit to discriminate faulty and healthy operation. The table also shows that minimum values for IED and CBD are when the fault occurs at the midpoint while maximum values are attained for a fault close to both ends of the line. Fig. 14 shows the parabolic trend of the IED and CBD metrics. This validates the potential of developing a mathematical-based approach to identify the fault location within a TL based on the proposed technique.

5 Practical applications

This section is aimed at validating the robustness of the proposed technique through its application on a practical case study as well as a large interconnected power system.

5.1 Practical case study

In August 2019, a L–G fault took place on phase B of the 220 kV, 80 km TL shown in Fig. 15. During normal operation, a 10.87 MW

© The Institution of Engineering and Technology 2020

Authorized licensed use limited to: Electricity Generating Authority of Thailand. Downloaded on November 09,2020 at 08:24:32 UTC from IEEE Xplore. Restrictions apply.

Table 8 Classification metrics based on extracted image features

Metric	Healthy	25 km	50 km	75 km	100 km	125 km
IED	—	37.8	11.4	0.91	7.3	31.1
CBD	—	44.68	13.53	1.12	8.46	36.53
RMS	1.49	28.2	9.6	0.84	6.6	23.5

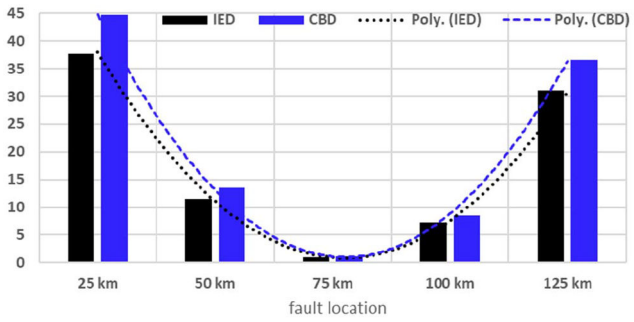

Fig. 14 *Impact of L–G fault on classification metrics*

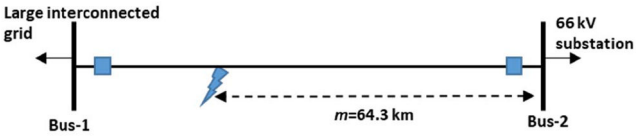

Fig. 15 *Practical fault in a 220 kV TL*

Table 9 recorded voltages and currents at both ends during fault

Phase	Bus-1		Bus-2	
	Voltage, kV	Current, kA	Voltage, kV	Current, kA
phase-A	141.5∠9.9°	0.11∠161.4°	126.2∠0.2°	0.11∠11.6°
phase-B	8.7∠ − 163.8°	0.16∠166.3°	68.2∠ − 56°	0.28∠163.6°
phase-C	143.5∠109.6°	0.08∠179.4°	127∠119.6°	0.07∠3.4°

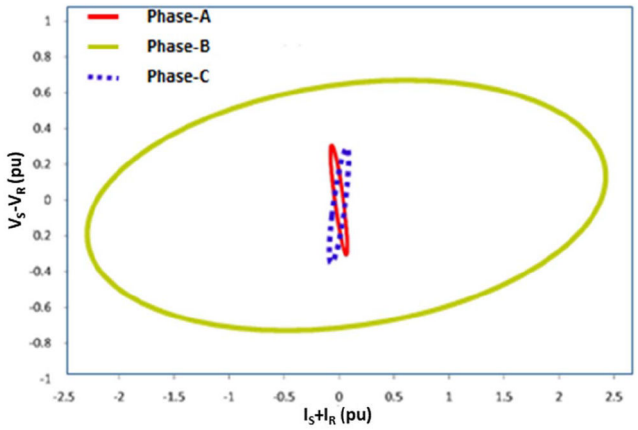

Fig. 16 *Single L–G fault on phase-B of the practical case study*

Table 10 Geometrical dimensions for bolted L–G fault at different locations for the practical case study

Feature	Phase-A	Phase-B	Phase-C
g_1	0.04	4.94	0.04
g_2	0.08	1.34	0.09
g_3	0.64	4.71	0.65
g_4	0.63	4.52	0.64
θ	−1.4	0.08	1.41

active power flows from bus-2 to bus-1 with a line–line voltage of 220 kV and 0.89 lagging power factor at bus-1. When the fault occurs at $m = 64.3$ km, the two circuit breakers at the two ends of the line were tripped and isolated the faulty zone. Recorded currents and voltages at both ends of the line during the fault are recorded as shown in Table 9. As can be seen, the faulty phase exhibits the least voltage and maximum current at both ends of the line.

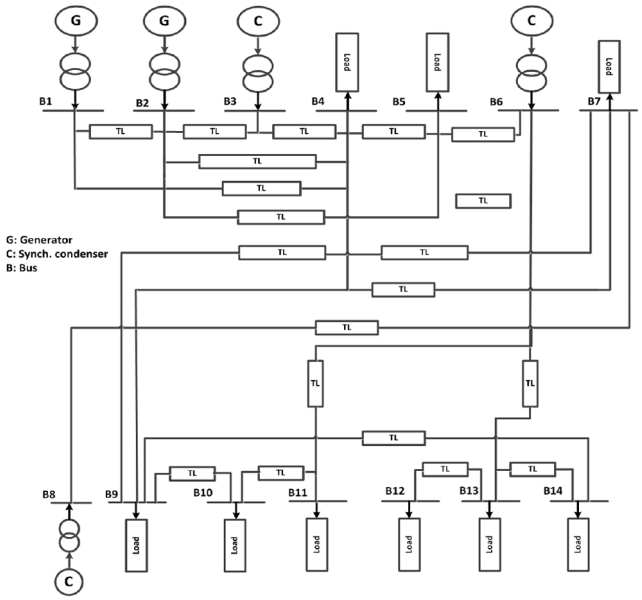

Fig. 17 *IEEE 14-bus system*

Data in Table 9 are converted to the pu values considering 220 kV and 100 MVA as base values. Instantaneous voltages and currents are sampled over one power cycle to plot the proposed ellipse for each phase as shown in Fig. 16. The proposed line elliptic plots in Fig. 16 reveal that the normal two phases (A and C) provide symmetrical but mirrored characteristics. The faulty phase (B) exhibits a substantial increase in the entire area due to the L–G fault. Table 10 shows the extracted geometrical dimensions for the ellipses of the three phases. As the reference data of this practical case study are not available, geometrical dimensions of the healthy phases (A or C), which have almost similar features except in the mirrored angles of rotation can be taken as a reference set. Considering phase-A data as a reference set, the IED and CBD for phase-B are 6.4 and 8.97, respectively. By applying interpolation using these two metrics and the corresponding values in Fig. 14, the fault location is estimated to be at a distance of 65.4 km from bus-2 with an estimation error of −1.71%. It is to be noted that this comparison is not very accurate due to the different topologies of the studied networks in both cases along with the unknown fault impedance in the practical case study. For the practical implementation of this technique, various network topologies have to be investigated with different fault scenarios and locations to improve estimation accuracy.

5.2 Large interconnected power system

To assess the applicability of the proposed technique for large interconnected power systems, the IEEE 14-bus system shown in Fig. 17 is simulated and solved using Matlab/Simulink to get the line currents and bus voltages at different operating conditions [26]. The proposed technique is applied on four TLs in the system; these are: TLs connecting buses 4–5, buses 6–11, buses 10–11, and buses 13 and 14. The proposed *V–I* characteristics of these lines are constructed using the voltage and current data at both ends of each line during normal operating conditions as shown in Fig. 18. As can be observed from the obtained results, each TL exhibits a

© The Institution of Engineering and Technology 2020

Authorized licensed use limited to: Electricity Generating Authority of Thailand. Downloaded on November 09,2020 at 08:24:32 UTC from IEEE Xplore. Restrictions apply.

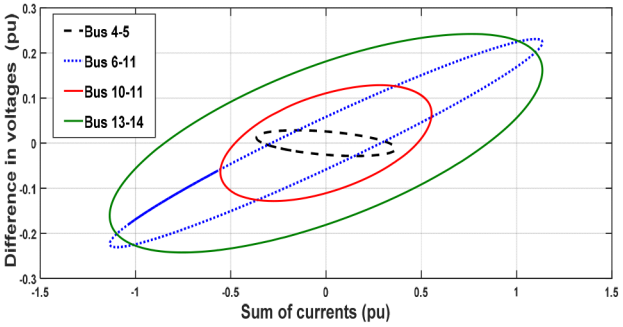

Fig. 18 *Fingerprints of four selected lines of the IEEE 14-bus system*

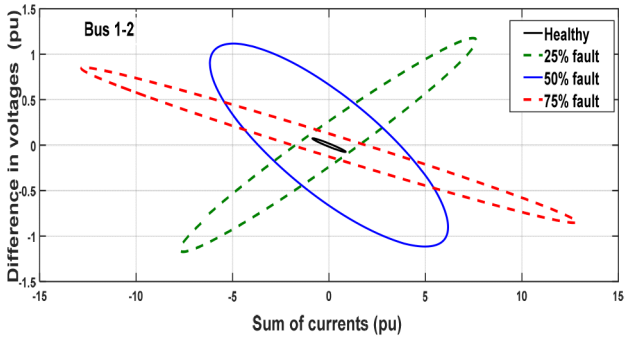

Fig. 19 *Healthy and L–G faulty loci for TL connecting buses 1 and 2 in the IEEE 14-bus system*

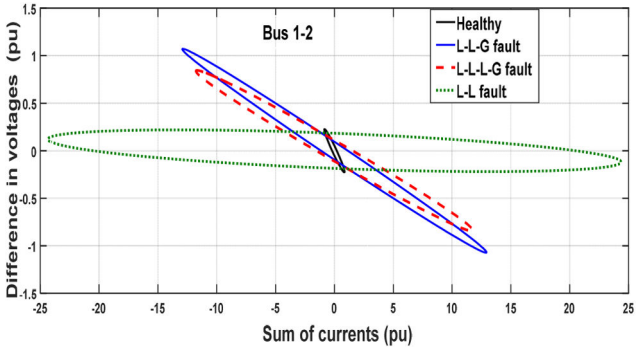

Fig. 20 *Loci of different faults at the middle of the TL connecting buses 1 and 2 in the IEEE 14-bus system*

unique figure print, which is mainly attributed to the different parameters of these lines.

A bolted single L–G fault is simulated at different locations (25, 50, and 75% from bus-1) of the TL connecting buses 1 and 2 in the IEEE 14-bus system. The obtained loci for the investigated line during normal operation and the L–G fault are shown in Fig. 19. Compared to the healthy signature, it can be seen that the faulty signatures are of good agreement with the obtained results in Fig. 5 in terms of the direction of rotation and the ellipse entire area. This confirms the effectiveness of the proposed technique for identifying fault locations in complex systems.

To show the ability of the proposed technique to detect and discriminate other types of TL faults as detailed in [13], three different types of faults are simulated in the middle of the line connecting buses 1 and 2 in the IEEE 14-bus system. These are double-line to ground (L–L–G), three-line to ground (L–L–L–G) and line to line (L–L) faults. As can be seen from the obtained loci in Fig. 20, each fault type will have a unique impact on the proposed line signature which enables the proposed technique to identify the type and location of various line faults.

Similar to other double-sided-based fault locating techniques, the proposed method calls for synchronised measurements of the instantaneous three-phase voltages and currents at both ends of the line through PMU and GPS. If these resources are not available, power flow analysis may be performed on the available data of the investigated system.

6 Conclusion

The feasibility of employing TL voltage–current characteristic to identify fault location and detect abnormal events within power lines is investigated. Simulation results show that the proposed technique is applicable for compensated, uncompensated, and hybrid-connected lines, which provide a privilege to this technique over existing industry practice that includes travelling wave and impedance methods. Each fault location has a unique impact on the proposed line fingerprint in terms of rotational angle, entire area, focus point, and major axis length. Unlike existing fault locating and protection techniques, the proposed method can detect high-impedance faults and abnormal events in real-time. The threshold value based on the RMS of the extracted features can be employed to discriminate faulty conditions from the normal line operation. On the other hand, fault location can be identified based on individual image features such as entire area and major axis length or some classification metrics including IED and CBD. The results of the practical case study in this paper reveal the practical feasibility of the proposed technique. However, further research along with practical validation should be conducted to attest to the commercial application of this technique.

7 References

[1] Liang, H., Liu, Y., Sheng, G., *et al.*: 'Reproduction methodology for single phase-to-ground faults in overhead transmission lines', *IEEE Access*, 2017, **5**, pp. 17403–17413

[2] Elkalashy, N.I., Kawady, T.A., Khater, W.M., *et al.*: 'Unsynchronized fault-location technique for double-circuit transmission systems independent of line parameters', *IEEE Trans. Power Deliv.*, 2016, **31**, (4), pp. 1591–1600

[3] Abd El-Ghany, H.A., Azmy, A.M., Abeid, A.M.: 'A general travelling-wave based scheme for locating simultaneous faults in transmission lines', *IEEE Trans. Power Deliv.*, 2020, **35**, (1), pp. 130–139, doi: 10.1109/TPWRD.2019.2931178

[4] Das, S., Santoso, S., Gaikwad, A., *et al.*: 'Impedance-based fault location in transmission networks: theory and application', *IEEE Access*, 2014, **2**, pp. 537–557

[5] Electric Power Research Institute, EPRI: 'Future inspection of overhead transmission lines', Technical Update, May 2008, pp. 1–88

[6] Magnago, F., Abur, A.: 'Fault location using wavelets', *IEEE Trans. Power Deliv.*, 1998, **13**, pp. 1475–1480

[7] 'IEEE guide for determining fault location on AC transmission and distribution lines', IEEE Std C37.114-2014 (Revision of IEEE Std C37.114-2004), 30 January 2015, pp. 1–76

[8] Bo, Z.Q., Weller, G., Redfern, M.A.: 'Accurate fault location technique for distribution system using fault-generated high-frequency transient voltage signals', *IEE Proc., Gener. Transm. Distrib.*, 1999, **146**, (1), pp. 73–79

[9] Lotfifard, S., Kezunovic, M., Mousavi, M.J.: 'A systematic approach for ranking distribution systems fault location algorithms and eliminating false estimates', *IEEE Trans. Power Deliv.*, 2013, **28**, (1), pp. 285–293

[10] Eriksson, L., Saha, M.M., Rockefeller, G.D.: 'An accurate fault locator with compensation for apparent reactance in the fault resistance resulting from remore-end infeed', *IEEE Trans. Power Appar. Syst.*, 1985, **PAS-104**, (2), pp. 423–436

[11] Takagi, T., Yamakoshi, Y., Yamaura, M., *et al.*: 'Development of a new type fault locator using the one-terminal voltage and current data', *IEEE Power Eng. Rev.*, 1982, **PER-2**, pp. 59–60

[12] Kang, N., Liao, Y.: 'Double-circuit transmission line fault location with the availability of limited voltage measurements', *IEEE Trans. Power Deliv.*, 2012, **27**, (1), pp. 325–336

[13] Abu-Siada, A., Mir, S.: 'A new on-line technique to identify fault location within long transmission lines', *Eng. Fail. Anal.*, 2019, **105**, pp. 52–64

[14] Abu-Siada, A., Islam, S.: 'A novel on-line technique to detect power transformer winding faults', *IEEE Trans. Power Deliv.*, 2012, **27**, (2), pp. 849–857

[15] Thomas, G.B., Finney, R.L.: '*Calculus and analytic geometry*' (Addison-Wesley, Reading, MA, 1996, 9th edn.)

[16] Aljohani, O., Abu-Siada, A.: 'Application of digital image processing to detect short circuit turns in power transformers using frequency response analysis', *IEEE Trans. Ind. Inf.*, 2016, **12**, (6), pp. 2062–2073

[17] Abu-Siada, A., Aljohani, O.: 'Detecting incipient radial deformations of power transformer windings using polar plot and digital image processing', *IET Sci. Meas. Technol.*, 2018, **12**, (4), pp. 492–499

[18] Gonzalez, R.C.: '*Digital image processing*' (Pearson, Upper Saddle River, NJ, USA, 2008)

[19] Canny, J.: 'A computational approach to edge detection', *IEEE Trans. Pattern Anal. Mach. Intell.*, 1986, **PAMI-8**, (6), pp. 679–698

[20] Wang, B., Fan, S.: 'An improved CANNY edge detection algorithm'. Proc. 2nd Int. Workshop on Computer Science and Engineering, Qingdao, People's Republic of China, 2009, pp. 497–500

[21] Aljohani, O., Abu-Siada, A.: 'Application of DIP to detect power transformers axial displacement and disk space variation using FRA polar plot signature', *IEEE Trans. Ind. Inf.*, 2017, **13**, (4), pp. 1794–1805

[22] McAndrew, A.: 'An introduction to digital image processing with Matlab notes for SCM2511 image processing', School of Computer Science and

© The Institution of Engineering and Technology 2020

Authorized licensed use limited to: Electricity Generating Authority of Thailand. Downloaded on November 09,2020 at 08:24:32 UTC from IEEE Xplore. Restrictions apply.

Mathematics, Victoria University Technology, Melbourne, Vic., Australia, 2004, pp. 1–264
[23] Chandola, V., Banerjee, A., Kumar, V.: 'Anomaly detection: a survey', *ACM Comput. Surv.*, 2009, **41**, pp. 1–72
[24] Farmer, R.G., Childers, C.V., Agrawa, B.L.*, et al.*: 'Second benchmark model for computer simulation of subsynchronous resonance', *IEEE Trans. Power Appar. Syst.*, 1985, **PAS-104**, pp. 1057–1066
[25] Tzelepis, D., Fusiek, G., Dyśko, A.*, et al.*: 'Novel fault location in MTDC grids with non-homogeneous transmission lines utilizing distributed current sensing technology', *IEEE Trans. Smart Grid*, 2018, **9**, (5), pp. 5432–5443
[26] Anderson, P.M., Fouad, A.A. (Eds.): '*Power system control and stability*' (IEEE Press, John Wiley and Sons Inc. Publication, USA, 2003)

© The Institution of Engineering and Technology 2020

Authorized licensed use limited to: Electricity Generating Authority of Thailand. Downloaded on November 09,2020 at 08:24:32 UTC from IEEE Xplore. Restrictions apply.